

# A Roche Model for Uniformly Rotating Rings

Stefan Horatschek<sup>\*</sup> and David Petroff<sup>\*</sup>

*Theoretisch-Physikalisches Institut, University of Jena, Max-Wien-Platz 1, 07743 Jena, Germany*

29 October 2018

## ABSTRACT

A Roche model for describing uniformly rotating rings is presented and the results are compared with numerical solutions to the full problem for polytropic rings. In the thin ring limit, the surfaces of constant pressure including the surface of the ring itself are given in analytic terms, even in the mass-shedding case.

**Key words:** gravitation – methods: analytical – hydrodynamics – equation of state – stars: rotation.

## 1 INTRODUCTION

A uniformly rotating star with a sufficiently soft equation of state can be described approximately using the Roche model (Roche 1873). In this model the matter is treated as a test fluid in a  $1/r$ -potential, i.e. one considers the whole mass of the star to be concentrated at the centre. By doing so, self-gravitating effects of the outer mass shells are neglected. Such Roche models have been considered, especially in the mass-shedding limit, by Zel'dovich & Novikov (1971); Shapiro & Shibata (2002). For polytropes with indices  $n \gtrsim 2.5$  this approximation yields results that differ by less than about a percent from their correct values (Meinel et al. 2008). Whereas most analytical solutions to figures of equilibrium describe bodies with constant mass density (e.g. the Maclaurin spheroids, Jacobi ellipsoids, etc.), the Roche model is very useful because it is applicable to non-homogeneous matter.

Aside from spheroidal figures of equilibrium, there exist configurations with toroidal topology. Such rings have been studied both analytically (Kowalewsky 1885; Poincaré 1885a,b,c; Dyson 1892, 1893; Ostriker 1964b; Petroff & Horatschek 2008) and numerically (Wong 1974; Eriguchi & Sugimoto 1981; Eriguchi & Hachisu 1985; Hachisu 1986; Ansorg et al. 2003b; Fischer et al. 2005).

Here we apply the basic idea of the Roche model to rings. Thus, we do not choose to have the test fluid rotate in the field of a point mass, but in that of a circular line of mass with constant linear mass density. In addition to the mass, we thus also have to specify the radius of the circle.

For the comparison of the solutions of the Roche model with those of the full problem for polytropes, we use a multi-domain spectral program, much like the one described in Ansorg et al. (2003a) and a similar one tailored to Newtonian bodies with toroidal topologies (see Ansorg & Petroff 2005 for more information).

## 2 THE ROCHE MODEL WITH A RING SOURCE

### 2.1 Basic Equations

If we use cylindrical coordinates  $(\varrho, z, \varphi)$ , then the gravitational potential of a circular line centred on the axis of mass  $M$  and radius  $b$  reads

$$U = -\frac{GM}{\pi} \int_0^\pi \frac{d\varphi}{\sqrt{b^2 + \varrho^2 + z^2 - 2b\varrho \cos \varphi}} \quad (1)$$

$$= -\frac{2GM}{\pi \sqrt{(b + \varrho)^2 + z^2}} K\left(\frac{2\sqrt{b\varrho}}{\sqrt{(b + \varrho)^2 + z^2}}\right), \quad (2)$$

where  $G$  is the gravitational constant and  $K$  denotes the complete elliptic integral of the first kind,

$$K(k) := \int_0^{\pi/2} \frac{d\theta}{\sqrt{1 - k^2 \sin^2 \theta}}. \quad (3)$$

Sometimes it will be convenient to use the polar-like coordinates  $r$  and  $\chi$  defined by

$$\varrho = b - r \cos \chi \quad \text{and} \quad z = r \sin \chi. \quad (4)$$

For a test fluid rotating uniformly with the angular velocity  $\Omega$ , Euler's equation can be written as

$$\nabla \left( U + h - \frac{1}{2} \Omega^2 \varrho^2 \right) = 0, \quad (5)$$

where  $h$  is defined by

$$h := \int_0^p \frac{dp'}{\mu(p')}, \quad (6)$$

and where  $p$  is the pressure,  $\mu$  the mass density and  $U$  the potential given above<sup>1</sup>. We integrate (5) and get

$$U + h - \frac{1}{2} \Omega^2 \varrho^2 = V_0, \quad (7)$$

<sup>\*</sup> E-mail: S.Horatschek@tpi.uni-jena.de (SH);  
D.Petroff@tpi.uni-jena.de (DP)

<sup>1</sup> For isentropic matter,  $h$  is simply the specific enthalpy.

where  $V_0$  is the constant of integration. Evaluating this equation at the surface of the ring, along which the function  $h$  vanishes, then leads to

$$U_s - \frac{1}{2}\Omega^2 \varrho^2 \Big|_s = V_0. \quad (8)$$

Via this equation, the surface of the ring, described by  $r_s = r_s(\chi)$  or  $z_s = z_s(\varrho)$ , and thus the ratio of inner and outer radius  $\varrho_i$  and  $\varrho_o$

$$A := \frac{\varrho_i}{\varrho_o}, \quad (9)$$

are given implicitly for prescribed  $M$ ,  $b$ ,  $\Omega^2$  and  $\varrho_o$ . Analogously, equation (7) can be used to find surfaces of constant  $h$ .

In what follows, we simplify the equations by introducing the dimensionless quantities

$$\frac{\bar{r}}{r} = \frac{\bar{b}}{b} = \frac{\bar{\varrho}}{\varrho} = \frac{\bar{z}}{z} = \frac{1}{\varrho_o}, \quad (10a)$$

$$\frac{\bar{\Omega}^2}{\Omega^2} = \frac{\bar{\varrho}_o^3}{GM}, \quad \frac{\bar{U}}{U} = \frac{\bar{V}_0}{V_0} = \frac{\bar{h}}{h} = \frac{\bar{\varrho}_o}{GM}, \quad (10b)$$

which implies  $\bar{\varrho}_i = A$  and  $\bar{\varrho}_o = 1$ . In the dimensionless versions of the above equations,  $GM$  cancels out. Except for two scaling constants (e.g.  $M$  and  $\varrho_o$ ), two parameters are necessary to describe a ring in the Roche model (e.g.  $\bar{b}$  and  $\bar{\Omega}^2$ ).

## 2.2 Mass-Shedding Configurations

Of particular interest are configurations at the mass-shedding limit. In this limit, a fluid particle at the outer rim rotates with the Kepler frequency, which means that the gravitational force is balanced by the centrifugal force alone – the pressure gradient vanishes. For the squared angular velocity at the mass-shedding limit we find

$$\bar{\Omega}_{\text{ms}}^2 = \frac{\partial \bar{U}}{\partial \bar{\varrho}} \Big|_{\bar{\varrho}=1, \bar{z}=0}. \quad (11)$$

With the potential (2) this gives

$$\bar{\Omega}_{\text{ms}}^2 = \frac{2E(\bar{b})}{\pi(1-\bar{b}^2)}, \quad (12)$$

where  $E$  denotes the complete elliptic integral of the second kind,

$$E(k) := \int_0^{\frac{\pi}{2}} \sqrt{1 - k^2 \sin^2 \theta} d\theta. \quad (13)$$

Contrary to the general case, only one parameter is free, the other one is fixed by equation (11).

Mass-shedding configurations have a cusp at the outer rim<sup>2</sup>, and we will now calculate the associated angle. At the surface, the quantity

$$V := U - \frac{1}{2}\Omega^2 \varrho^2 \quad (14)$$

is constant, see (8), which means that along the surface we have

$$0 = \frac{d^2 V}{d\varrho^2} = V_{,\varrho\varrho} + 2V_{,\varrho z} \frac{dz_s}{d\varrho} + V_{,zz} \left( \frac{dz_s}{d\varrho} \right)^2 + V_{,z} \frac{d^2 z_s}{d\varrho^2}, \quad (15)$$

<sup>2</sup> One can easily show that a configuration with a cusp must be at the mass-shedding limit. The converse statement, that mass-shedding configurations have a cusp, can be proved if one makes the very reasonable assumption that the pressure does not increase for increasing values of  $z$  in the upper half-space (Pähtz 2007).

where a comma indicates partial differentiation. The equatorial symmetry implies that first derivatives with respect to  $z$  vanish at  $z = 0$ , thus leading to

$$\varrho = \varrho_o, z = 0 : \quad \frac{dz_s(\varrho)}{d\varrho} = \sqrt{-\frac{V_{,\varrho\varrho}}{V_{,zz}}} = \sqrt{\frac{\Omega_{\text{ms}}^2 - U_{,\varrho\varrho}}{U_{,zz}}}. \quad (16)$$

Hence the full angle is

$$\begin{aligned} \delta &= 2 \arctan \sqrt{\frac{\Omega_{\text{ms}}^2 - U_{,\varrho\varrho}}{U_{,zz}}} \Big|_{\varrho=\varrho_o, z=0} \\ &= 1 - \frac{2(1-\bar{b}^2)E(\bar{b})}{(1-\bar{b}^2)K(\bar{b}) - 2E(\bar{b})}, \end{aligned} \quad (17)$$

cf. Fig. 4.

## 2.3 The Shape of the Surface

To treat both mass-shedding configurations and the general case, we parametrize the angular velocity by

$$\Omega^2 = \alpha \Omega_{\text{ms}}^2, \quad \alpha \in [0, 1]. \quad (18)$$

This choice of  $\alpha$  arises from the fact that the mass-shedding limit ( $\alpha = 1$ ) poses an upper bound for the angular velocity and a solution to (8) can be found for arbitrarily small  $\Omega^2$ .

Evaluating (8) at the point ( $\bar{\varrho} = \bar{\varrho}_o = 1, \bar{z} = 0$ ) yields

$$\bar{V}_0 = -\frac{1}{\pi} \left[ \frac{\alpha E(\bar{b})}{1-\bar{b}^2} + 2K(\bar{b}) \right] \quad (19)$$

and at the point ( $\bar{\varrho} = \bar{\varrho}_i = A, \bar{z} = 0$ ) gives

$$\bar{V}_0 = -\frac{1}{\pi} \left[ \frac{\alpha A^2 E(\bar{b})}{1-\bar{b}^2} + \frac{2}{b} K\left(\frac{A}{b}\right) \right]. \quad (20)$$

Requiring that both expressions for  $V_0$  agree leads to

$$K(\bar{b}) = \frac{1}{b} K\left(\frac{A}{b}\right) - \frac{\alpha(1-A^2)E(\bar{b})}{2(1-\bar{b}^2)}. \quad (21)$$

At an arbitrary surface point ( $\bar{\varrho}, \bar{z}_s(\bar{\varrho})$ ) we get

$$\begin{aligned} \bar{V}_0 &= -\frac{1}{\pi} \left[ \frac{\alpha \bar{\varrho}^2 E(\bar{b})}{1-\bar{b}^2} + \right. \\ &\quad \left. \frac{2}{\pi \sqrt{(\bar{b} + \bar{\varrho})^2 + \bar{z}_s^2}} K\left(\frac{2\sqrt{\bar{b}\bar{\varrho}}}{\sqrt{(\bar{b} + \bar{\varrho})^2 + \bar{z}_s^2}}\right) \right]. \end{aligned} \quad (22)$$

Together with (19) this is an implicit equation for the surface function  $\bar{z}_s(\bar{\varrho})$  or  $\bar{r}_s(\chi)$ . Unfortunately this function cannot be found in analytic terms, however it is not difficult to handle it numerically. Furthermore, it will be treated analytically for thin rings in the next subsection.

For a prescribed  $\alpha$ , the requirement  $A \geq 0$  means that (21) can only be satisfied for  $\bar{b}$  larger than some minimal value. It turns out that smaller values of  $\bar{b}$  no longer describe rings, but spheroidal figures. In this case, (20) and (21) must be replaced by

$$\bar{\varrho} = 0, \bar{z} = \bar{z}_p : \quad \bar{V}_0 = -\frac{1}{\sqrt{\bar{b}^2 + \bar{z}_p^2}} \quad (23)$$

and

$$K(\bar{b}) = \frac{\pi}{2\sqrt{\bar{b}^2 + \bar{z}_p^2}} - \frac{\alpha E(\bar{b})}{2(1-\bar{b}^2)}, \quad (24)$$

where  $\bar{z}_p = z_p/\varrho_0$  denotes the dimensionless polar radius, in other words, the ratio of the polar to the equatorial radius. The transition from spheroidal to toroidal topologies is described when  $\bar{z}_p = 0$  or equivalently  $A = 0$ . In the limit  $\bar{b} \rightarrow 0$ , the potential (2) becomes that of a point mass  $M$  at the star's centre and one recovers the 'standard' Roche model, cf. Appendix A.

## 2.4 Thin Rings

In the thin ring limit in which  $A \rightarrow 1$ , clearly  $\bar{b}$  also tends to 1. This limit is of particular interest, especially since a self-gravitating thin ring is also tractable to analytical methods (Kowalewsky 1885; Poincaré 1885b,c,d; Dyson 1892, 1893; Ostriker 1964b; Petroff & Horatschek 2008). By expanding the surface function

$$\bar{r}_s(\chi) = \sum_{i=1}^{\infty} s_i(\chi) (1 - \bar{b})^i \quad (25)$$

about the thin ring limit  $\bar{b} \rightarrow 1$ , equation (8) yields

$$0 = \alpha[1 + s_1(\chi) \cos \chi] + \ln s_1(\chi), \quad (26)$$

which can be solved by using the Lambert W function, which fulfils the equation  $W(x)e^{W(x)} = x$ :

$$s_1(\chi) = e^{-W(\alpha e^{-\alpha \cos \chi}) - \alpha} = \frac{W(\alpha e^{-\alpha \cos \chi})}{\alpha \cos \chi}. \quad (27)$$

For  $\alpha \rightarrow 0$ , we find  $s_1(\chi) = 1$  meaning that the cross-section tends toward a circle for  $\bar{b} \rightarrow 1$ . For  $\alpha = 1$  (and only for this value),  $s_1(\chi)$  is not differentiable at the point  $\chi = \pi$  although both one-sided derivatives exist. One finds

$$\lim_{\chi \uparrow \pi} \frac{ds_1(\chi)}{d\chi} = -\lim_{\chi \downarrow \pi} \frac{ds_1(\chi)}{d\chi} = 1, \quad (28)$$

which implies that the angle at this point is  $\delta = \pi/2$ , which can also be derived from (17) in the limit  $\bar{b} \rightarrow 1$ . A series of pictures showing the shapes of  $s_1(\chi)$  for various values of  $\alpha$  can be found in Fig. 1. Higher terms  $s_i(\chi)$  from the series (25) can be found iteratively and contain powers of  $\ln(1 - \bar{b})$ .

To calculate surfaces of constant  $h$ ,  $\bar{r}_h(\chi)$ , we can easily generalize the above calculation. Like (25), we expand these surfaces about the thin ring limit

$$\bar{r}_h(\chi) = \sum_{i=1}^{\infty} t_i^h(\chi) (1 - \bar{b})^i. \quad (29)$$

As mentioned above, the function  $h$  vanishes at the surface, i.e.  $\bar{r}_s(\chi) = \bar{r}_0(\chi)$  and  $s_i = t_i^0$ . Equation (5) then gives

$$0 = \alpha \left[ 1 + t_1^h(\chi) \cos \chi \right] + \ln t_1^h(\chi) + \pi \bar{h}, \quad (30)$$

and thus

$$t_1^h(\chi) = e^{-W(\alpha e^{-\alpha - \pi \bar{h}} \cos \chi) - \alpha - \pi \bar{h}} = \frac{W(\alpha e^{-\alpha - \pi \bar{h}} \cos \chi)}{\alpha \cos \chi}. \quad (31)$$

This function is depicted in Fig. 2 for  $\alpha = 1$  and various values of  $\bar{h}$ . For large values of  $\bar{h}$ , we have

$$\lim_{\bar{h} \rightarrow \infty} t_1^h(\chi) e^{\alpha + \pi \bar{h}} = 1 \quad (32)$$

meaning that the curves of constant  $h$  become circular as the source is approached. In the limit  $\alpha \rightarrow 0$  we find that

$$h = -\frac{GM}{b} \frac{1}{\pi} \ln t, \quad t \in (0, 1] \quad (33)$$

only depends on the coordinate  $t := \bar{r}/(1 - \bar{b})$ , but not on  $\chi$ .

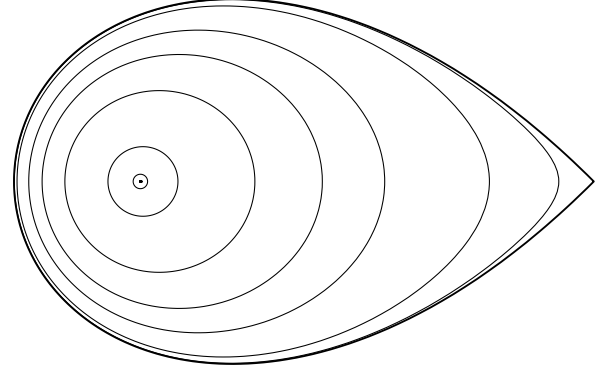


**Figure 2.** Lines of constant pressure (corresponding to constant  $\bar{h}$ ) are shown for the mass-shedding ring in the thin ring limit. The function  $t_1^h(\chi)$  with  $\alpha = 1$  is depicted for various values of  $\bar{h}$  in polar coordinates, where the axis of rotation is to the left of the cross-section and infinitely far away. The surface, which corresponds to  $\bar{h} = 0$ , is precisely  $s_1(\chi)$  and can also be found in Fig. 1. The values of  $\bar{h}$  starting from the surface and moving inward are 0, 0.001, 0.01, 0.05, 0.1, 0.2, 0.5 and 1. The value of  $\bar{h}$  tends to infinity at the point, where the source is located.

## 3 COMPARISON WITH THE FULL PROBLEM

The comparison of the Roche model with the full problem requires the identification of various physical quantities. Whereas  $M$ ,  $\Omega$ ,  $V_0$ ,  $A$  and  $z_s(\varrho)$  are clearly defined in both, the value of  $b$ , which describes the location of the singular source in the Roche model, is not defined in the full problem. There, we choose  $b$  to be the position of the centre of mass of a meridional cross-section of the ring.

The Roche model contains two scaling parameters, which can be 'eliminated' by using the dimensionless quantities introduced in (10), and two physical parameters. On the other hand, for a given equation of state, the full problem is determined by specifying a scaling parameter and only one physical parameter. When comparing a specific Roche model with a solution to the full problem, one thus has freedom as to how to make such a comparison. One can, for example, choose to have  $\bar{b}$  and  $\bar{\Omega}$  agree and then compare  $\bar{V}_0$ ,  $A$  and the shape of the surface. One could also choose to have  $\bar{b}$  and  $A$  agree and then compare  $\bar{\Omega}$ ,  $\bar{V}_0$  and the shape of the surface.

There must be some well-defined way of choosing the additional parameter in the Roche model if the full problem is to tend to it in some limit. Let us consider rings made up of matter obeying the equation of state

$$p = K\mu^{1+1/n}, \quad (34)$$

i.e. polytropes, where  $K$  is the polytropic constant and  $n$  the polytropic index. If such rings are expanded about the limit  $A \rightarrow 1$ , then a solution results, the first few terms of which provide a good approximation to the full problem over some range of values for  $A$  (Ostriker 1964b; Petroff & Horatschek 2008). This range of values shrinks to the single point  $A = 1$  in the limit  $n \rightarrow \infty$ , i.e. in the 'isothermal limit'. This means that the 'isothermal' rings must be infinitely thin. Because we expect that only such rings can be treated arbitrarily well in the Roche model, we do have a well defined way of choosing the 'additional parameter': namely  $A = 1$ . The one remaining free physical parameter, e.g.  $\alpha$ , corresponds to the single physical parameter one has in the full solution and interpolates between mass-shed rings and those with circular cross-sections. We thus expect that there exist isothermal (and necessarily infinitely thin) rings with non-circular cross-sections, cf. Fig. 1.

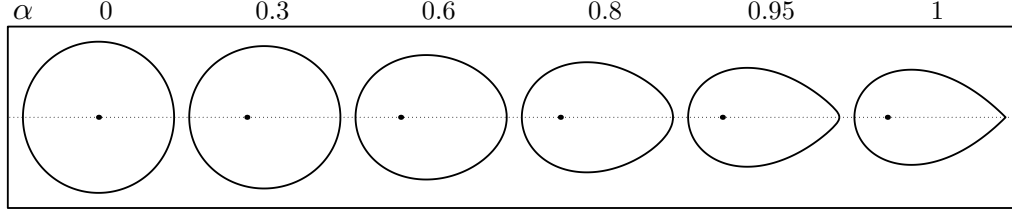


**Figure 1.** Cross-sections of rings in the thin ring limit scaled such that the horizontal extent of each is equal. The function  $s_1(\chi)$  is depicted for various values of  $\alpha$  in polar coordinates, where the axis of rotation is to the left of each cross-section and infinitely far away. The dots indicate the origin, where the source of the potential is located.

Those with circular cross-sections were studied in the papers mentioned in the last paragraph and the results presented here must coincide with those for  $\alpha = 0$ . Indeed expression (148) for the potential and (35) with (151) for the angular velocity in Ostriker (1964b) together with  $\beta^{-1} \gg \xi \gg 1$  show that  $\Omega^2 b^2$  is negligible compared to  $U$ , as implied by  $\alpha = 0$  and (18). Furthermore, the logarithmic behaviour (33) can be recovered from (120), (122), (125) and (127) in Ostriker (1964b)<sup>3</sup> (see also Ostriker 1964a; Petroff & Horatschek 2008)

$$h_{\text{iso}} = h_c - 2K \ln \left( 1 + \frac{\xi^2}{8} \right), \quad \xi \in [0, \infty). \quad (35)$$

In expression (33) the function  $h$  diverges at the centre  $t = 0$  and the surface is located at the finite radius  $t = 1$ , whereas in (35) the corresponding function remains finite at the centre  $\xi = 0$ , but diverges at the surface  $\xi \rightarrow \infty$ . To compare the expressions for  $h$ , we thus take a derivative in order to eliminate the physically irrelevant constant and consider only the regular portion of the  $t$ -interval,  $t > 0$ , which corresponds to infinite values of  $\xi$ . This leads to

$$t \frac{dh}{dt} = -\frac{GM}{\pi b} \quad (36)$$

and

$$\lim_{\xi \rightarrow \infty} \xi \frac{dh_{\text{iso}}}{d\xi} = -4K, \quad (37)$$

which can indeed be seen to be in agreement upon taking into account

$$GM = 4\pi K b, \quad (38)$$

see (146) and the definitions (97) in Petroff & Horatschek (2008). The situation is analogous to that in the spherically symmetric case as discussed in Appendix A.

If we depart from the thin ring limit, then the comparison with numerical solutions to the full problem of a uniformly rotating, self-gravitating ring allows us to address the particularly important question of how good the Roche model is. Tables 1 and 2 show how this model converges toward the full solution for polytropic rings as the polytropic index  $n$  is increased. The first of these provides a comparison of rings with the radius ratio  $A = 0.7$  and the second for mass-shedding configurations ( $\alpha = 1$  for the Roche model). In both cases, the value of  $\bar{b}$  for the Roche model was chosen to agree with the numerical one. The second column,  $\kappa$ , gives an indication of how concentrated the mass is. If we consider the cross-section of a ring, and define the two points in the equatorial plane at which the density falls off to half of its maximal value

$$\mu(\varrho_a, z = 0) = \mu(\varrho_b, z = 0) = \frac{\mu_{\text{max}}}{2}, \quad \varrho_b > \varrho_a, \quad (39)$$

**Table 1.** Comparison between polytropic rings with  $A = 0.7$  and the corresponding Roche configuration with the same  $\bar{b}$ .  $\Delta$  denotes the difference between the values of the Roche configuration and the values of the full solution.

$n$	$\kappa$	$\bar{b}$	$\Delta\Omega/\Omega_{\text{num}}$	$\Delta V_0/V_{0 \text{ num}}$
1.0	$6.3 \times 10^{-1}$	$8.48 \times 10^{-1}$	$2.6 \times 10^{-2}$	$7.4 \times 10^{-3}$
1.5	$4.9 \times 10^{-1}$	$8.46 \times 10^{-1}$	$1.9 \times 10^{-2}$	$6.0 \times 10^{-3}$
3.0	$2.7 \times 10^{-1}$	$8.42 \times 10^{-1}$	$8.2 \times 10^{-3}$	$3.1 \times 10^{-3}$
5.0	$1.3 \times 10^{-1}$	$8.34 \times 10^{-1}$	$2.6 \times 10^{-3}$	$1.2 \times 10^{-3}$
7.0	$7.2 \times 10^{-2}$	$8.26 \times 10^{-1}$	$8.6 \times 10^{-4}$	$4.7 \times 10^{-4}$

then  $\kappa$  is defined to be the ratio of the distance between these two points to the total width of the ring's cross-section

$$\kappa := \frac{\varrho_b - \varrho_a}{\varrho_o - \varrho_i}. \quad (40)$$

Only for  $\kappa \ll 1$  is the Roche model expected to give good results. We find that  $\kappa \lesssim 0.2$  for polytropic rings with  $n \gtrsim 3$ . Such polytropes always have values for the radius ratio  $A \gtrsim 0.45$ , which implies that Roche models with a smaller radius ratio do not provide a particularly close approximation to any toroidal polytrope.

The shapes of cross-sections of mass-shedding rings for various polytropic indices are plotted in Fig. 3. Here, the differences that arise due to different prescriptions of the parameters are evident for small values of the polytropic index. When  $A$  is chosen to coincide between the Roche model and the full solution, then the two surfaces do not differ appreciably, even for  $n = 1$ . The radius ratio itself, and consequently the shape, is quite different for a Roche model with  $\bar{b}$  as prescribed from the solution to the full problem with  $n = 1$ . These differences vanish as  $n$  is increased and the two prescriptive choices converge to the full solution as they must.

Fig. 4 provides an interesting comparison between mass-shedding configurations for polytropes and the Roche model. The angle  $\delta$  of the cusp as given by (17) is plotted over the whole interval  $\bar{b} \in [0, 1]$  as a solid line. This curve is compared to two distinct polytropic mass-shedding sequences generated by varying the polytropic index  $n$ . The dotted line describes rings and merges together with that of the Roche model in the thin ring limit, i.e. for  $\bar{b} \rightarrow 1$ . On the other hand, the dashed line describes (spheroidal) stars and merges together with that of the Roche model for  $\bar{b} \rightarrow 0$ . The change in topologies in the Roche model from toroidal to spheroidal takes place for  $\bar{b} \approx 0.56$  as can be calculated by solving for  $\bar{b}$  in (21) with  $A = 0$  and  $\alpha = 1$ .

In summary, we can say that as with stars, the Roche model presented here for rings is seen to yield a very good approximation to the full problem in many cases. Moreover, it presumably provides exact results in the appropriate limit and offers new solutions that had not been found using perturbative approaches.

<sup>3</sup> Equation (122) in Ostriker (1964b) should read  $\rho = \lambda e^{-\Psi} = \rho_0 e^{-\Psi}$ .

**Table 2.** Comparison between polytropic rings in mass-shedding and the corresponding Roche configuration with the same  $\bar{b}$ .  $\Delta$  denotes the difference between the values of the Roche configuration and the values of the full solution.

$n$	$\kappa$	$\bar{b}$	$\Delta A/A_{\text{num}}$	$\Delta\Omega/\Omega_{\text{num}}$	$\Delta\delta/\delta_{\text{num}}$	$\Delta V_0/V_{0\text{ num}}$
1.0	$5.3 \times 10^{-1}$	$5.77 \times 10^{-1}$	$-3.7 \times 10^{-1}$	$-3.8 \times 10^{-2}$	$2.7 \times 10^{-2}$	$-4.1 \times 10^{-2}$
1.5	$4.0 \times 10^{-1}$	$6.04 \times 10^{-1}$	$-1.0 \times 10^{-1}$	$-2.0 \times 10^{-2}$	$1.3 \times 10^{-2}$	$-2.1 \times 10^{-2}$
3.0	$2.1 \times 10^{-1}$	$6.53 \times 10^{-1}$	$-1.2 \times 10^{-2}$	$-3.9 \times 10^{-3}$	$2.1 \times 10^{-3}$	$-4.4 \times 10^{-3}$
5.0	$1.1 \times 10^{-1}$	$6.92 \times 10^{-1}$	$-2.0 \times 10^{-3}$	$-7.7 \times 10^{-4}$	$3.4 \times 10^{-4}$	$-8.8 \times 10^{-4}$
7.0	$5.7 \times 10^{-2}$	$7.20 \times 10^{-1}$	$-4.7 \times 10^{-4}$	$-2.0 \times 10^{-4}$	$7.8 \times 10^{-5}$	$-2.4 \times 10^{-4}$

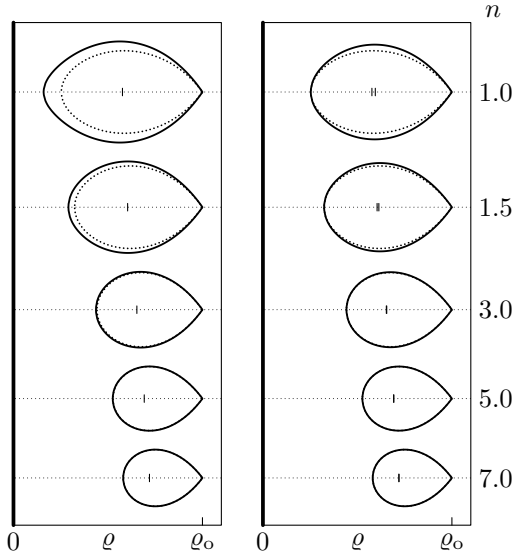


**Figure 3.** Comparison between the cross-sections of polytropic rings at the mass-shedding limit (dotted lines) and those of the corresponding Roche configurations, i.e. with  $\alpha = 1$  (solid lines). In the left panels the Roche model was chosen such that  $\bar{b}$  agrees with the numerical value, whereas in the right panels, the values of  $A$  were chosen to coincide. The ticks in the ‘centre’ indicate the values of  $\bar{b}$ . When  $A$  is prescribed (right panels), it turns out that  $\bar{b}_{\text{num}} < \bar{b}_{\text{Roche}}$ .

## ACKNOWLEDGMENTS

We are grateful to Reinhard Meinel for a careful reading of this paper. We also want to thank our referee, Yoshiharu Eriguchi, for his helpful comments. This research was funded in part by the Deutsche Forschungsgemeinschaft (SFB/TR7-B1).

## REFERENCES

- Ansorg M., Kleinwächter A., Meinel R., 2003a, *Astron. Astrophys.*, 405, 711  
 Ansorg M., Kleinwächter A., Meinel R., 2003b, *Mon. Not. R. Astron. Soc.*, 339, 515  
 Ansorg M., Petroff D., 2005, *Phys. Rev. D*, 72, 024019  
 Dyson F. W., 1892, *Philos. Trans. R. Soc. London, Ser. A*, 184, 43  
 Dyson F. W., 1893, *Philos. Trans. R. Soc. London, Ser. A*, 184, 1041  
 Eriguchi Y., Hachisu I., 1985, *Astron. Astrophys.*, 148, 289  
 Eriguchi Y., Sugimoto D., 1981, *Prog. Theor. Phys.*, 65, 1870  
 Fischer T., Horatschek S., Ansorg M., 2005, *Mon. Not. R. Astron. Soc.*, 364, 943  
 Hachisu I., 1986, *Astrophys. J. Suppl. Ser.*, 61, 479  
 Kowalewsky S., 1885, *Astronomische Nachrichten*, 111, 37

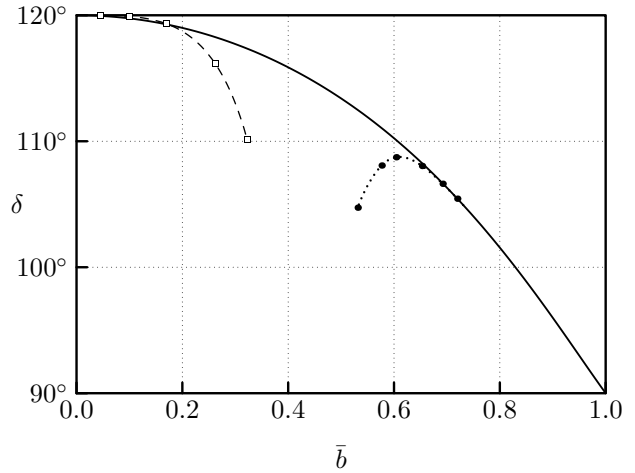


**Figure 4.** The angle  $\delta$  of the cusp for the mass-shedding configurations in the Roche model (solid line) is compared with the numerical result for polytropic rings (dotted line) and polytropic spheroidal configurations (dashed line). The larger dots denote the ring configurations with  $n = 1/2, 1, 3/2, 3, 5$  and  $n = 7$ , where smaller values of  $n$  correspond to smaller values of  $\bar{b}$ , and the white squares denote the spheroidal configurations with  $n = 1/2, 1, 2, 3$  and  $n = 4$ , where larger values of  $n$  correspond to smaller values of  $\bar{b}$ . In the thin ring limit, where we expect that the Roche model provides arbitrarily good results to the full problem for ‘isothermal’ rings ( $n \rightarrow \infty$ ), we find  $\delta \rightarrow 90^\circ$ .

- Meinel R., Ansorg M., Kleinwächter A., Neugebauer G., Petroff D., 2008, *Relativistic Figures of Equilibrium*. Cambridge University Press, Cambridge  
 Ostriker J., 1964a, *Astrophys. J.*, 140, 1056  
 Ostriker J., 1964b, *Astrophys. J.*, 140, 1067  
 Pähz T., 2007, *Untersuchungen des Mass-Shedding-Limits rotierender Flüssigkeiten in Newtonscher und Einsteinscher Gravitationstheorie*, Diplomarbeit, Friedrich-Schiller-Universität Jena  
 Petroff D., Horatschek S., 2008, *Mon. Not. R. Astron. Soc.*, 389, 156  
 Poincaré H., 1885a, *Acta mathematica*, 7, 259  
 Poincaré H., 1885b, *C. R. Acad. Sci.*, 100, 346  
 Poincaré H., 1885c, *Bull. Astr.*, 2, 109  
 Poincaré H., 1885d, *Bull. Astr.*, 2, 405  
 Roche É., 1873, *Mém. de la section des sciences, Acad. des sciences et lettres de Montpellier*, 1, 235  
 Shapiro S. L., Shibata M., 2002, *Astrophys. J.*, 577, 904  
 Wong C. Y., 1974, *Astrophys. J.*, 190, 675  
 Zel’dovich Y. B., Novikov I. D., 1971, *Relativistic Astrophysics*. Vol. 1, The University of Chicago Press, Chicago

**APPENDIX A: THE STANDARD ROCHE MODEL**

As mentioned in the introduction, the Roche model with a  $1/r$ -potential was discussed by Roche (1873); Zel'dovich & Novikov (1971); Shapiro & Shibata (2002) and provides a unique surface function describing a mass-shedding star. To derive this function, we follow Meinel et al. (2008) and begin by writing down equation (8) with the potential  $U_s$  of a point mass

$$V_0 + \frac{GM}{\sqrt{\varrho^2 + z_s(\varrho)^2}} + \frac{1}{2}\Omega^2 \varrho^2 = 0. \quad (\text{A1})$$

By considering the point  $\varrho = 0$ , we can relate the constant  $V_0$  to the polar radius  $z_p$

$$V_0 = -\frac{GM}{z_p}. \quad (\text{A2})$$

For mass-shedding stars, the relation

$$\left. \frac{\partial U}{\partial \varrho} \right|_{\varrho=\varrho_0, z=0} = \varrho_0 \Omega^2, \quad (\text{A3})$$

where  $\varrho_0$  is the equatorial radius, leads to

$$GM = \varrho_0^3 \Omega^2, \quad (\text{A4})$$

and the surface equation (A1) becomes

$$z_p \left( \frac{1}{\sqrt{\varrho^2 + z^2}} + \frac{\varrho^2}{2\varrho_0^3} \right) = 1. \quad (\text{A5})$$

Evaluating this expression at the equator,  $z = 0$ , tells us that for mass-shedding fluids in the Roche model, the radius ratio

$$\frac{z_p}{\varrho_0} = \frac{2}{3} \quad (\text{A6})$$

follows. With this relationship, the curve describing the fluid's surface can be rewritten as

$$z_s = \frac{\sqrt{4\varrho_0^2 - \varrho^2} (\varrho_0^2 - \varrho^2)}{3\varrho_0^2 - \varrho^2}. \quad (\text{A7})$$

It then follows that

$$\lim_{z \downarrow 0} \frac{dz_s}{d\varrho} = -\sqrt{3}, \quad (\text{A8})$$

which means the interior angle of the mass-shedding cusp is  $120^\circ$  (see Fig. 4 for  $\bar{b} \rightarrow 0$ ).

In general, the Roche model is expected to approach the full solution when the matter is arbitrarily concentrated. For static polytropes, the full problem leads to the Lane-Emden equation, which turns out to describe arbitrarily concentrated matter if  $n = 5$ . We shall now show the agreement between these stars and the results given by the Roche model.

In the static case, the Roche model gives

$$h = GM \left( \frac{1}{R} - \frac{1}{R_0} \right), \quad R \in (0, R_0] \quad (\text{A9})$$

and thus

$$R^2 \frac{dh}{dR} = -GM. \quad (\text{A10})$$

The solution to the full problem is

$$\mu_5 = \mu_c \left( 1 + \frac{\xi^2}{3} \right)^{-5/2}, \quad \xi \in [0, \infty) \quad (\text{A11})$$

and thus

$$h_5 = 6K\mu_5^{1/5}, \quad (\text{A12})$$

where

$$\xi = \frac{x}{l}, \quad l^2 = \frac{3K}{2\pi G\mu_c^{4/5}} \quad (\text{A13})$$

is the dimensionless radius and  $x$  the true radius. The surface extends out to infinity and since the regular portion of the  $R$ -interval,  $R > 0$ , corresponds to infinite values of the radius  $x$ , we consider

$$\lim_{x \rightarrow \infty} x^2 \frac{dh_5}{dx} = -6\sqrt{3}Kl\mu_c^{1/5}. \quad (\text{A14})$$

Calculating the mass for the full problem,

$$GM = 4\pi G \int_0^\infty \mu_5 x^2 dx = 4\pi\sqrt{3}l^3\mu_c = 6\sqrt{3}Kl\mu_c^{1/5}, \quad (\text{A15})$$

shows the equivalence of (A10) and (A14).